UHASSELT
KNOWLEDGE IN ACTION

# Faculteit Wetenschappen

master in materiomics

**_Masterthesis_**

## *The design and optimization of flexible OLEDs*

**Robin Quanten**
Scriptie ingediend tot het behalen van de graad van master in materiomics

**PROMOTOR :**
Prof. dr. ir. Koen VANDEWAL
Prof. dr. Wouter MAES

2023
2024

---

UHASSELT
KNOWLEDGE IN ACTION

**www.uhasselt.be**
Universiteit Hasselt
Campus Hasselt:
Martelarenlaan 42 | 3500 Hasselt
Campus Diepenbeek:
Agoralaan Gebouw D | 3590 Diepenbeek

# Faculteit Wetenschappen

master in materiomics

***Masterthesis***

***The design and optimization of flexible OLEDs***

**Robin Quanten**

Scriptie ingediend tot het behalen van de graad van master in materiomics

**PROMOTOR :**

Prof. dr. ir. Koen VANDEWAL

Prof. dr. Wouter MAES

Academic year 2023-2024

# The design and optimization of flexible OLEDs

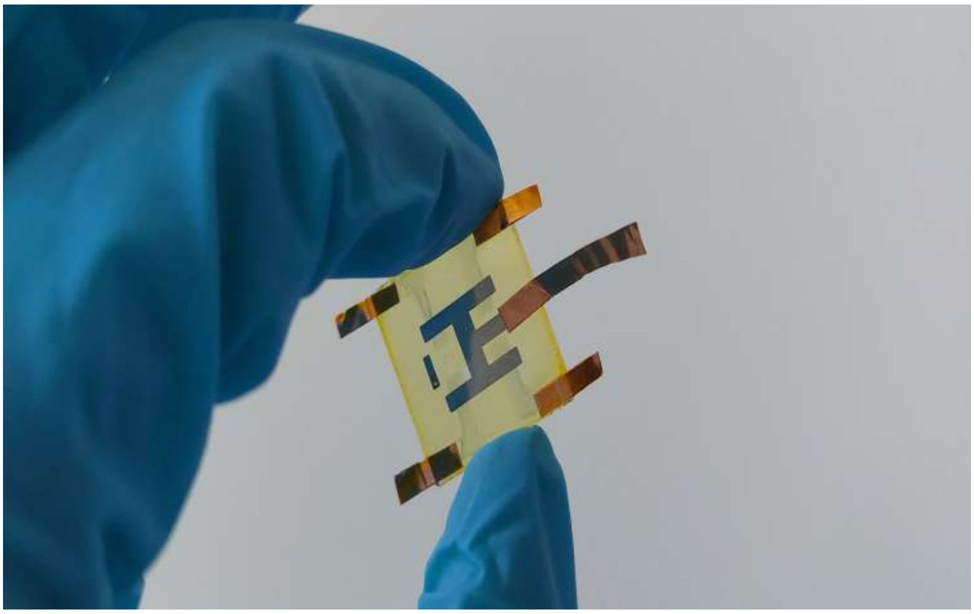

Robin Quanten (1848639)
Master in Materiomics
Prof. Dr. Ir. Koen Vandewal
Mr. Bram Bijnens

# The design and optimization of flexible OLEDs

Student: *Robin Quanten*[1,*]
Promotor: *Prof. Dr. Ir. Koen Vandewal*[1]
Copromotor: *Prof. Dr. Wouter Maes*[2]
Supervisor: *Mr. Bram Bijnens*[1]

[1] Organic-Optoelectronics (OOE), Wetenschapspark 1, 3590 Diepenbeek, Belgium.
[2] Design & Synthesis of Organic Semiconductors (DSOS), Agoralaan Gebouw F, 3590 Diepenbeek, Belgium.
*Email: robin.quanten@student.uhasselt.be

**Keywords**:
organic light-emitting diode, parylene-C, poly(3,4- ethylene-dioxythiophene)-poly(styrene sulfonate), ultra-flexible devices

**Abstract**:

Organische lichtgevende diodes (OLED's) bieden tal van voordelen voor elektronische toepassingen, waaronder uitzonderlijke flexibiliteit. Het ontwikkelen van ultradunne, volledig functionele lichtgevende apparaten die zeer flexibel zijn, is essentieel voor onderzoek naar beeldschermen en biomedische sensoren. Verdere optimalisatie van OLED's is echter cruciaal om hun volledige potentieel te benutten. Dit onderzoek richt zich op het ontwikkelen van een nieuwe procedure om flexibele OLED's te maken. Het hoofddoel is een grondig begrip te krijgen van de complexe interacties tussen de OLED-componenten. De apparaten zijn ontworpen met minimale lagen om de complexiteit te verminderen: poly(2-chloor-p-xylyleen) (paryleen-C)/poly(3,4-ethyleen-dioxythiofeen)-poly(styreensulfonaat) (PEDOT:PSS)/Super Yellow (SY)/ polyethyleenimine-ethoxylaat (PEIE)/Aluminium. Een methode is ontwikkeld om paryleen-C direct te patronen met PEDOT:PSS vanuit een oplossing via spincoating, terwijl ook de geleidbaarheid van PEDOT:PSS wordt verbeterd voor gebruik als elektrode. Het ontwerp van het apparaat is geoptimaliseerd met simulatiehulpmiddelen en experimenteel onderzoek, wat resulteerde in de meest efficiënte configuratie. De resulterende apparaten hebben een gemiddelde externe kwantumefficiëntie (EQE) van 0,5% en vertonen een matige degradatie, waarbij de EQE daalt tot 60% van de oorspronkelijke waarden. De vrijstaande OLED's vertonen opmerkelijke flexibiliteit en behouden hun lichtgevende eigenschappen tijdens gebruik in omgevingsomstandigheden.

**Abstract**:

Organic light-emitting diodes (OLEDs) offer numerous benefits for electronic applications, especially their exceptional flexibility. Developing ultra-thin, fully functional light-emitting devices that withstand deformation can significantly impact various fields, such as displays and biomedical sensors. However, further optimizing OLED designs is crucial to unlock their full potential across various applications. This research aims to develop a novel approach to creating flexible OLEDs. The primary goal is to understand the complex interactions among the OLED components thoroughly. The devices are designed with minimal layers to reduce complexity: poly(2-chloro-p-xylylene) (parylene-C)/poly(3,4-ethylene-dioxythiophene)-poly(styrene sulfonate) (PEDOT:PSS )/Super Yellow (SY)/polyethylenimine-ethoxylated (PEIE)/Aluminum. A method is established for patterning parylene-C with PEDOT:PSS directly from a solution via spin coating while also enhancing the conductivity of PEDOT:PSS for use as an electrode. The device design is optimized through simulation tools and experimental investigations, resulting in the most efficient configuration. The resulting devices have an average external quantum efficiency (EQE) of 0.5% and exhibit moderate degradation, with EQEs dropping to 60% of their initial values. The free-standing OLEDs demonstrate remarkable flexibility while maintaining their light-emitting properties during operation in ambient conditions.

# 1 Introduction

Organic Light-Emitting Diodes (OLEDs) currently represent a prominent field of research and have done so for several decades. This is primarily attributed to the unique properties of organic molecules that enable the development of devices characterized by flexibility, the potential for printing, high resolution, improved contrast ratios, and reduced weight, which were unattainable with preceding technologies [1] such as light-emitting diodes (LEDs) and liquid-crystal displays (LCDs). Due to these appealing properties, OLEDs have found their way into numerous applications. The most outstanding is their integration into displays for televisions, portable devices, and biomedical applications. Many companies and research facilities keep on improving the designs of these devices to achieve, among others, curved ultra-high definition TV screens [2], flexible, thin, wearable devices such as watches with high contrast [3], and light sources in pulse oximetry [4].

This profound interest in these light sources will ensure future endeavors to improve these previous applications. One of these properties, which is taken to a higher level, is the flexibility of the OLEDs. A recent example consisted of a very thin, flexible OLED rolled up into a catheter with a diameter of just 1,8 mm. This catheter was used as a photobiomodulation platform to treat particular areas of tubular organs utilizing phototherapeutics [5]. A different research group developed a patch consisting of a built-in OLED. This thin and flexible patch could be applied to a specific surface area of interest on a patient's skin to aid in phototherapeutic therapy for treating skin cancers [6].

However, these OLED devices can be designed to be more flexible and suitable for niche applications, such as the catheter mentioned above. This requires reevaluating the total design, as each layer will behave distinctly differently than in the more rigid OLED devices. The deformations imposed on this device will affect how well the light can be generated and the efficient escape of this light through constituent layers. Thus, it is essential to research how the increased flexibility influences the light outcoupling efficiency and how this can be improved. Previous research has investigated OLEDs on parylene-C substrates, providing high flexibility to these devices, with succes [7,8] using vacuum depositions techniques.

This thesis aimed to maximize an OLED's external quantum efficiencies (EQE) while retaining a high degree of flexibility to understand better the factors that dictate this device's performance. Parylene-C substrates provided the flexibility of these devices, so an effort was made to try and control the thicknesses of these substrates consistently via chemical vapor deposition (CVD) to produce identical substrates for these devices each time. Tuning the surface properties of parylene-C in very specific areas, combined with conductivity improvements of PEDOT:PSS resulted in highly conductive, fully transparent, and sharply defined PEDOT:PSS bottom electrodes on these substrates. A complete device was constructed on top according to materials and their parameters from the literature. It uses Super Yellow (SY) as the emissive layer, polyethyleneimine-ethoxylated (PEIE) as the electron transporting layer, and an aluminum electrode on top. The full device, apart from the parylene-C substrate and the top aluminum electrode, was deposited from spin coating. The resulting devices were characterized for their external quantum efficiencies (EQEs), IV characteristics, and degradation.

Furthermore, free-standing OLEDs were established and tested solely supported by the ultraflexible parylene-C substrate. Moreover, simulations were performed to identify possible problems in the design of these OLEDs that could negatively affect the light outcoupling efficiency. A possible improvement deducted from these simulations was the replacement of the aluminum top electrode with a fully organic one consisting of PEDOT:PSS. This potential improvement was attempted for implementation.

# 2 Results and discussion

## 2.1 Device architecture

The OLEDs were constructed as presented in **Figure 1**. These devices consisted of evaporated aluminum top electrodes. The thin polyethyleneimine-ethoxylated (PEIE) layer was the electron transporting layer (ETL) that reduced the electron transport barrier between the top electrode and the other layers. The fluorescent polymer Super Yellow (SY) was employed as the emissive layer. PEDOT:PSS with improved conductivity was used as a transparent and flexible bottom electrode. The substrate for the OLED stack was a transparent 2.5 µm parylene-C film, providing the necessary support for all upper layers and facilitating high flexibility, which will be discussed in the following section.

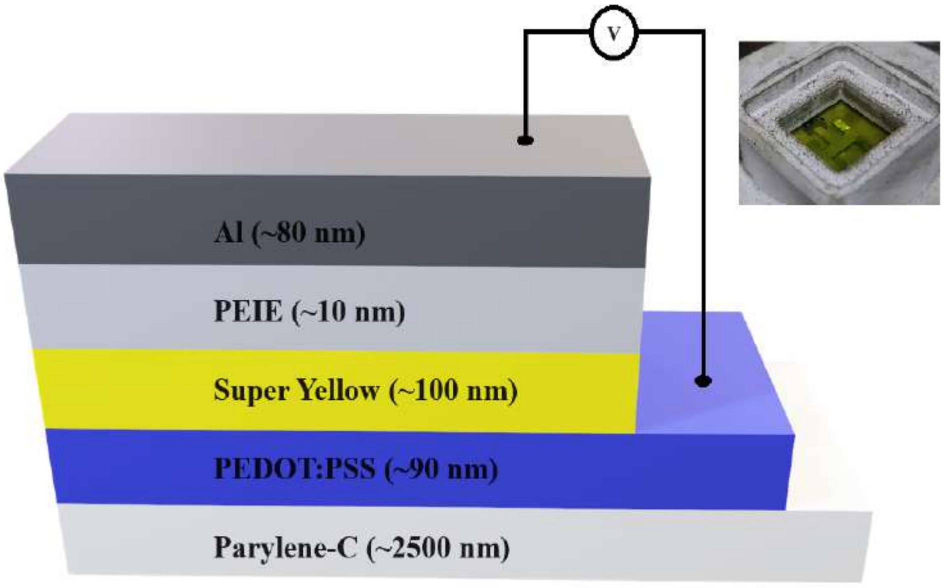

**Figure 1:** Device structure of OLEDs in this thesis, inset: picture of an operating OLED pixel.

## 2.2 Substrate optimization

Chemical vapor deposition (CVD) was used to deposit parylene-C reliably substrates with accurate control over their thickness. A calibration curve for the deposition apparatus was obtained by coating multiple glass substrates with varying masses of parylene-C pellets, and the resulting layer thicknesses were measured using a profilometer. **Figure 2a** shows this calibration curve from which it was deduced that each gram of parylene-C pellets loaded in the deposition apparatus would result in a layer of approximately 560 nm. The parylene-C films showed high transmission values (average 87%), which approached the values of quartz glass substrates

(91%) (**Figure 2b**). Thicker films did show thin film interference but solely dropped the average transmission to 86%. The most optimal thickness was 2.5 µm, as this would provide the best trade-off between transmission and film strength. A polyethylene glycol (PEG) sacrificial layer was added to the quartz glass substrate before CVD, aiming to improve the lift-off of this parylene-C film to obtain the free-standing OLEDs.

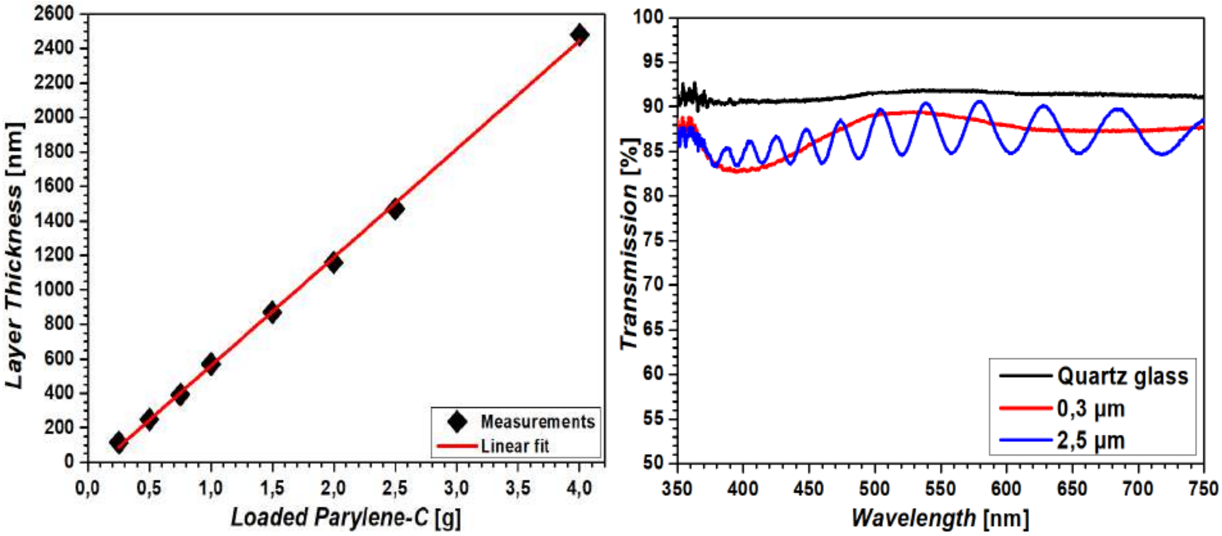

**(a)** **(b)**

**Figure 2:** (a) Thickness measurements for chemical vapor deposition-established parylene-C films as a function of loaded parylene-C pellets; (b) light transmission of quartz substrate and two parylene-C films differing in thickness.

## 2.3 Bottom electrode modification

PEDOT:PSS substituted indium tin oxide (ITO) as a flexible, transparent bottom electrode. PEDOT:PSS is an intrinsically semi-conducting polymer mixture in an aqueous solution that cannot adhere to hydrophobic surfaces, such as the parylene-C-coated substrates. An innovative method was developed in this research to treat the parylene-C substrate in specific areas, turning those areas hydrophilic [9, 10]. This was achieved by placing a mask for the desired PEDOT:PSS pattern on top of the parylene-C films during UV-ozone treatment. The exposed surfaces of the substrate would solely result in distinct hydrophilic areas on this film. The hydrophilic areas allow PEDOT:PSS adhesion upon spin coating, resulting in sharply defined patterns (**Appendix A**). The identical patterns for each OLED allow for consistent comparisons between different devices.

Further conductivity improvements are required to properly use this material as the bottom electrode for the OLED device, as pristine PEDOT:PSS films had resistances as high as 1500 kΩ. Different treatment methods and solvents were tested for their resulting conductivities, film morphologies, and light transmission (**Appendix B**), and compared to the literature [11–19] to determine the most optimal method for this device. Homogeneous PEDOT:PSS patterns were achieved after spin coating and subsequently received post-treatment with methanol or dimethyl sulfoxide (DMSO) [20–23], resulting in the lowest resistances of 1.1 kΩ and 0.7 kΩ, respectively. The post-treatment procedure involved administering 15 µl of these solvents to the individual PEDOT:PSS electrodes while annealing these electrodes on the hotplate at 120°C for 15 minutes. Introducing these highly polar solvents to the PEDOT:PSS electrodes induced changes on the molecular level for the interactions between the conducting PEDOT- and insulating PSS polymers, resulting in better charge transport over the films. The different solvents did not affect the light transmission of these PEDOT:PSS electrodes; thickness only had a slight influence (**Appendix B**).

## 2.4 Device characterization

All OLED devices were measured and characterized while still attached to the glass substrate. This will ensure proper measurements are taken and allow for consistent comparisons to determine their properties qualitatively.

### 2.4.1 External quantum efficiencies

External quantum efficiency (EQE) encompasses the performance of an OLED device and presents a quantitative manner in which OLEDs can be compared. The most conventional way to define this parameter is presented in equation 1 [24,25].

$$EQE = \frac{\#emitted\,photons}{\#injected\,charges} \tag{1}$$

The EQE can be subdivided into four different efficiencies, each contributing to the global EQE value. Equation 2 provides a more fundamental way to grasp the processes that determine the performance of these OLEDs.

$$EQE = \eta_{PLQY} * \eta_{S/T} * \eta_{rec} * \eta_{out} \tag{2}$$

$\eta_{PLQY}$ represents the ratio of the radiative decay rate from the excited state to the total decay rate, which consists of the sum of the radiative- and all non-radiative decay rates. $\eta_{S/T}$ symbolizes the number of singlet and triplet excited states that form upon the recombination of electrons and holes and, subsequently, will emit photons via fluorescence or phosphorescence, respectively. $\eta_{rec}$ is the recombination efficiency and indicates how well electrons and holes can recombine within the emissive layer. Lastly, $\eta_{out}$ embodies the outcoupling efficiency, which is strictly related to the device architecture in enabling the generated light from exiting the device in the desired direction. Achieving the highest possible efficiencies for these four factors will contribute to a significantly higher EQE, as each factor is multiplied by the other [24,25].

**Figure 3a** presents an overview of all the measured EQEs of the pixels for methanol- and DMSO-treated devices, which were relatively low, with, on average, 0.45% and 0.65%, respectively. The literature reported EQE values up to 5%, indicating that further improvements

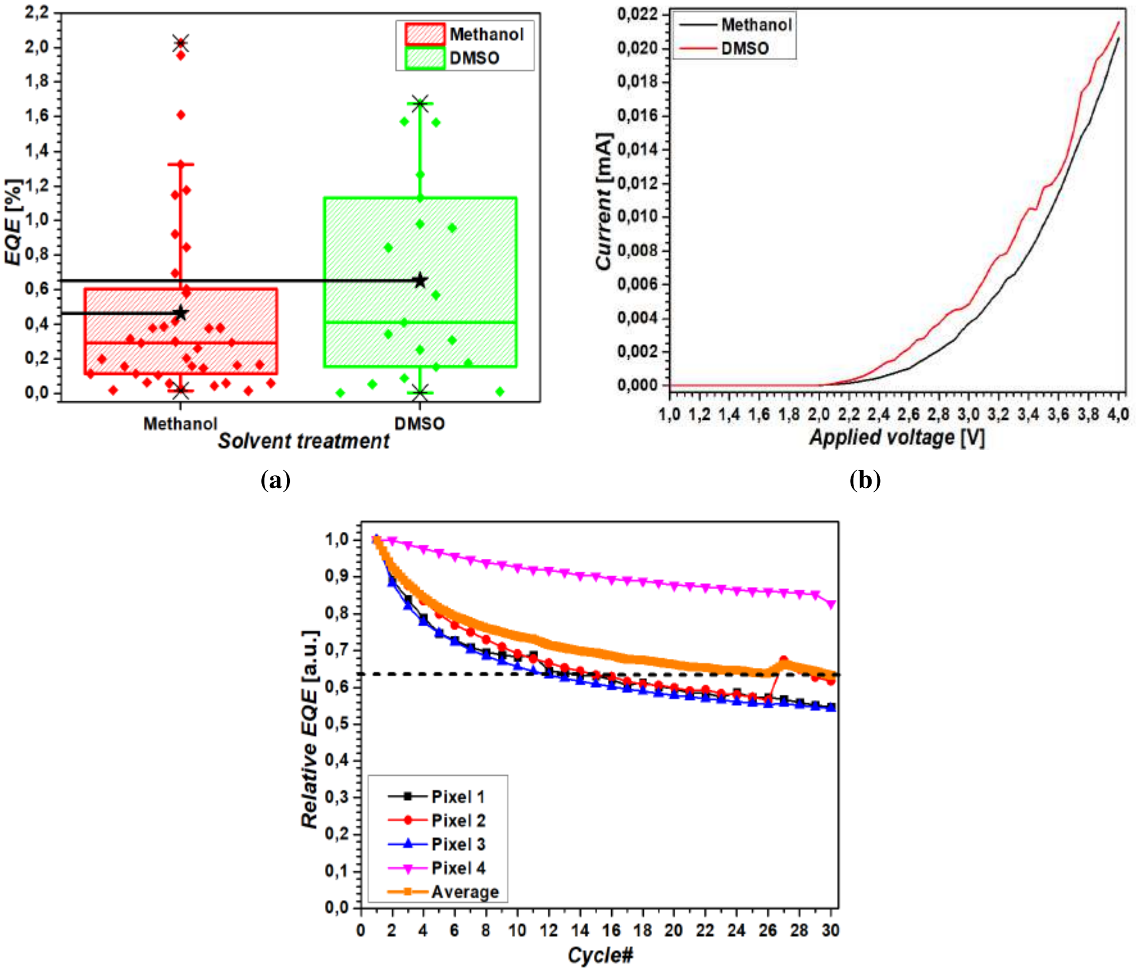

(a)

(b)

(c)

**Figure 3:** (a) Boxplot of EQE results for OLED devices treated with either methanol or DMSO. Stars indicate the average EQE values. The pixels of thirteen methanol-treated devices and six DMSO-treated devices were tested, and faulty pixels were omitted from these results; (b) IV-curves of methanol- and DMSO-treated pixels which showed an EQE of 0.4%; (c) Degradation results of four methanol-treated pixels, measurements performed via 30 subsequent voltage cycles from -0.5V to 5V and taking the EQE at 4V for each cycle to construct this plot.

should be achievable using Super Yellow [26–28]. However, few pixels reached an EQE above 1% and almost 2%. These higher EQEs could result from a few pixels with more optimal conditions for one or more constituent layers than the other more common pixels in these devices, culminating in better performances.

These low EQEs can be analyzed by combining the measured EQE data, computational models, and theory to determine the weak spots in the design of these OLEDs. **Table 1** summarizes the four efficiencies related to the current OLED concept necessary to determine the EQE.

**Table 1:** Efficiencies regarding architecture and emissive layer for OLED, with $\eta_{S/T}$ and $\eta_{PLQY}$ derived from literature [26–28] and $\eta_{out}$ from simulations in section 2.6. $\eta_{rec}$ obtained via combining measured EQE (0.45%) with three other efficiencies.

| $\eta_{rec}$ | $\eta_{S/T}$ | $\eta_{PLQY}$ | $\eta_{out}$ |
|---|---|---|---|
| 53-13% | 25% | 60% | 5-20% |

Due to spin statistics upon electron-hole recombination of these two 1/2-spin particles, 25% of the excited states end up in a singlet state (total spin 0) while the other 75% end up in triplet states (total spin 1). As SY is a fluorescent polymer, solely singlet excited states contribute to the light emission, losing the remaining 75% of excited states to non-radiative decay pathways. Moreover, other researchers had determined a $\eta_{PLQY}$ of about 60% in films, among the highest $\eta_{PLQY}$ reported values for fluorescent polymers [26–28]. These two efficiencies cannot be altered due to their inherent properties and thus would require different materials. Second- and third-generation OLED materials manage to use both singlet and triplet excited states to emit light via phosphorescence and thermally activated delayed fluorescence, respectively. These materials are often small-molecule-based, which is suitable for vacuum deposition techniques. This enables greater control over deposition conditions, resulting in much higher $\eta_{PLQY}$-values ranging from 70% to almost 100% [29–32]. With an identical device architecture, it would be reasonable to assume that the EQEs of these devices can achieve values of 1.8% up to 10%. The latter EQE value is achievable by optimizing the outcoupling efficiency to reach 20%, which, according to section 2.6, could be possible. This outcoupling can be further improved by utilizing evaporation techniques to deposit the organic emissive material, providing the ability to govern the dipole orientations within this layer.

Furthermore, the recombination efficiency can be tuned by varying the ETL thickness, shifting the recombination zone in the emissive layer, and improving the conductivity of the PEDOT:PSS electrode to prevent charge trapping. These latter potential improvements, combined with outcoupling efficiency simulation results in section 2.6, were implemented (section 2.7).

### 2.4.2 IV-characterization

**Figure 3b** and additional results in **Appendix C.1** showed that pixels with approximately equal EQEs had similar IV characteristics. Ohm's law indicated a resistance of 51.21 k$\Omega$ for methanol-treated pixels. The DMSO-treated pixel's resistance was approximately 53.09 k$\Omega$, indicating a slightly better conductivity for the former. Both solvents show significant differences in their properties, which profoundly influence their ability to tune the conductivity of PEDOT:PSS. Firstly, there is a difference in boiling temperature between the two solvents. DMSO has a significantly higher boiling temperature (189°C) than methanol (64°C) [33]; applying these solvents to the PEDOT:PSS film while at 120°C will result in much faster evaporation of methanol as compared to DMSO. Secondly, methanol is significantly more polar than DMSO, with values relative to water of 0.762 and 0.444 [33], respectively, thus influencing the PEDOT-PSS interactions in the electrode more.

It could be assumed that the changes that methanol can facilitate in a relatively shorter period due to its lower boiling point can be matched by DMSO over a longer time as a result of

DMSO's higher boiling point. This could be a possible explanation for the close match between both devices. Other explanations can still be found in the device architecture, such as the changes to the PEDOT:PSS' work function [34–36], which is not covered in this thesis.

### 2.4.3 Degradation

The stability of these flexible OLED devices is a crucial feature that must be assessed. To understand their ability to generate light over time, the stability of the devices was quantified by performing degradation tests, which consisted of subsequent voltage cycles from -0.5V to 5V. During these cycles, the changes to the device's performance were measured (**Figure 3c**). The pixels first showed a steep drop in EQE over the first six to eight cycles, after which a slight decrease in EQEs could be noticed. At the final cycles, the EQE did not change significantly, reaching an average EQE of about 60% of their initial value. More measurements are required to make concrete conclusions on the degradation of these pixels.

## 2.5 Proof-of-Concept: Free-standing OLED devices

The devices showed promising performances, which could be used to obtain free-standing devices from this proven OLED architecture. The main goal was to separate the OLED on the parylene-C substrate from the glass substrate onto which it had been constructed and verify whether generating light from these pixels in its free-standing form would be possible. This was an important test to assess whether these types of devices can be reliable enough for future endeavors toward specific applications for these highly flexible OLEDs.
The devices could be peeled off the quartz glass substrate, resulting in free-standing, flexible, thin OLEDs (**Figure 4a**). The films showed enough strength and flexibility to support these OLEDs during and after lift-off from the quartz glass substrates. The initial free-standing OLEDs' light emission was achieved by manually administering small traces of conductive silver paste onto the central metal electrode and the PEDOT:PSS electrodes in the corners. This paste consisted of silver nanoparticles suspended in acetone. The acetone would dissolve the upper organic layers until the PEDOT:PSS electrode. The PEDOT- and PSS polymers do not completely dissolve, resulting in a conductive path to which an external circuit could be connected to inject the required current (**Figure 4b**).
This technique, however, required applying tape to the edges of the OLED to apply the silver paste and properly connect them, resulting in semi-freestanding devices. Moreover, dissolving the OLED device aiming to make proper connections is not ideal and sometimes causes connection issues, thus rendering the devices unusable. Lastly, issues occurred with the stability of these devices during operation. Exposure to ambient air degrades the SY layer during operation. This results in a steady drop in current upon applying voltage to the pixels over time.

Copper strips were integrated into the OLED device to combat these issues and obtain a proper free-standing device. These strips were applied to the PEDOT:PSS bottom electrodes before spin-coating the upper layers. A final copper strip was applied to the upper Al-electrode before coating the devices with parylene-C via CVD; this ensured a complete encapsulation of the device to protect against humidity and oxygen in the environment **Figure 4c**. These devices did not require any additional steps to facilitate connections, as was the case with the previous design, and light could immediately be generated (**Figure 4d**). **Appendix D** shows additional images of free-standing devices regarding light-emission and flexibility.

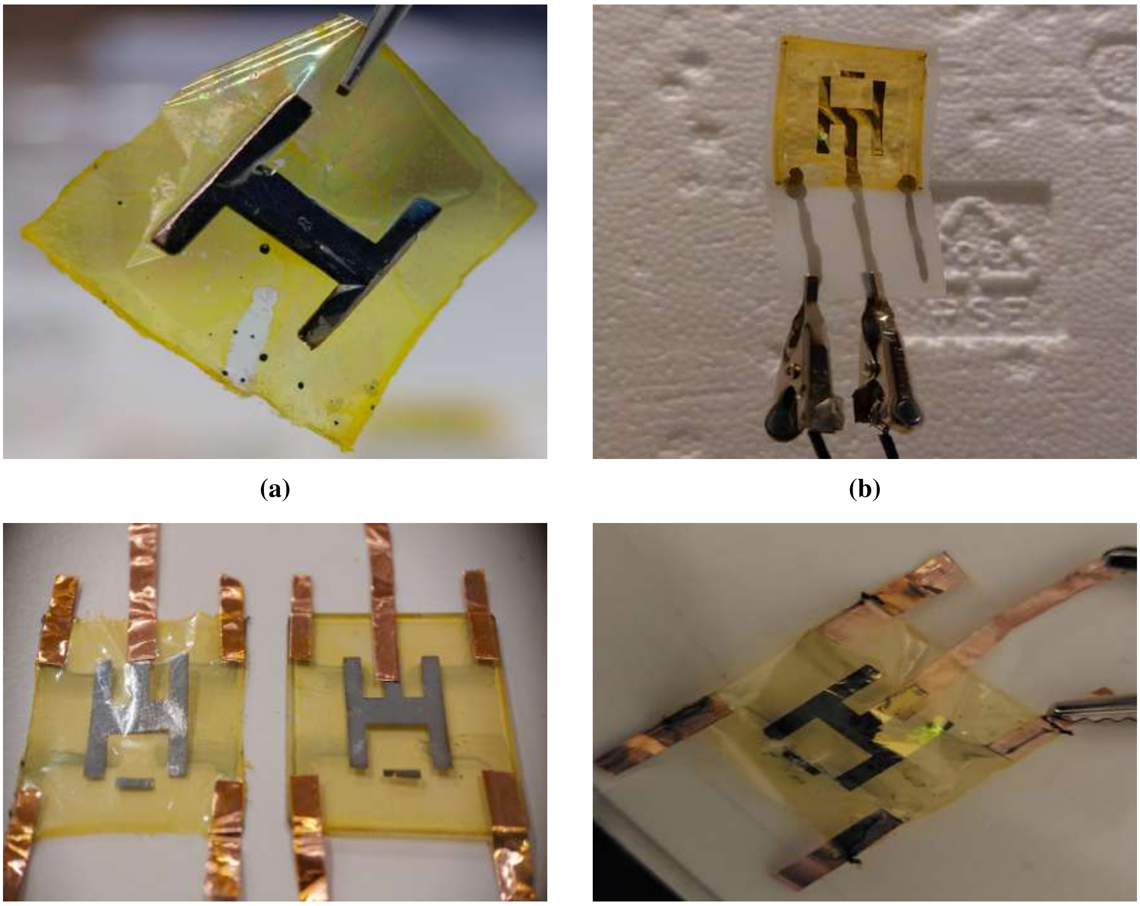

(a) (b) (c) (d)

**Figure 4:** Results of two iterations for free-standing devices, not-integrated- and integrated electrodes. (a) free standing OLED before applying silver paste and tape for facilitating connections, (b) externally applied connections with the light-emitting pixel at the bottom left of the device, (c) integrated copper films in device architecture to facilitate proper connections internally; left: free-standing OLED & right: OLED on glass substrate, (d) connected free-standing OLED with the light-emitting pixel in the top right.

However, this design still had its flaws, as it showed signs of degradation during operation, although at a noticeably slower rate, and had a turn-on voltage between 3.5V and 4V. Most crucially, the copper strips would often break the PEDOT:PSS pattern to which it had been stuck. As the device is put through the spin coating and displacements, these copper strips could bend and move, slightly breaking the PEDOT:PSS electrode underneath in the process, thus disrupting the connection. This could sometimes be verified by applying pressure to the point of overlap between the copper film and PEDOT:PSS, as this would instantly improve the current. Further research must address this problem, potentially via an additional annealing step or device pressing.

## 2.6 OLED simulations

Potential EQE losses were identified using Python simulations. These simulations were performed on 2D models, requiring the following input parameters: layer thicknesses, absorption coefficients and refractive indices of each layer, PLQY of the emissive layer, and the emission wavelength range. Though the simulation assumes homogeneous white light for these simulations, possible indications could be deducted from these results. The simulation iterated by increasing the electron-transporting layer (ETL) thickness (PEIE) to determine relative outcoupling efficiencies to air. The losses of generated light were categorized into three categories: surface-plasmon polaritons (SPP) as a result of light interactions with temporary excess charges on the aluminum electrode resulting in light guided along the organic-metal surface, waveguide (WG) modes are losses due to total internal reflection (TIR) resulting from reflection at the interfaces of the different stacks within the OLED, and substrate losses (Sub) are a consequence of TIR at the substrate-air and substrate-OLED interfaces [37–39].

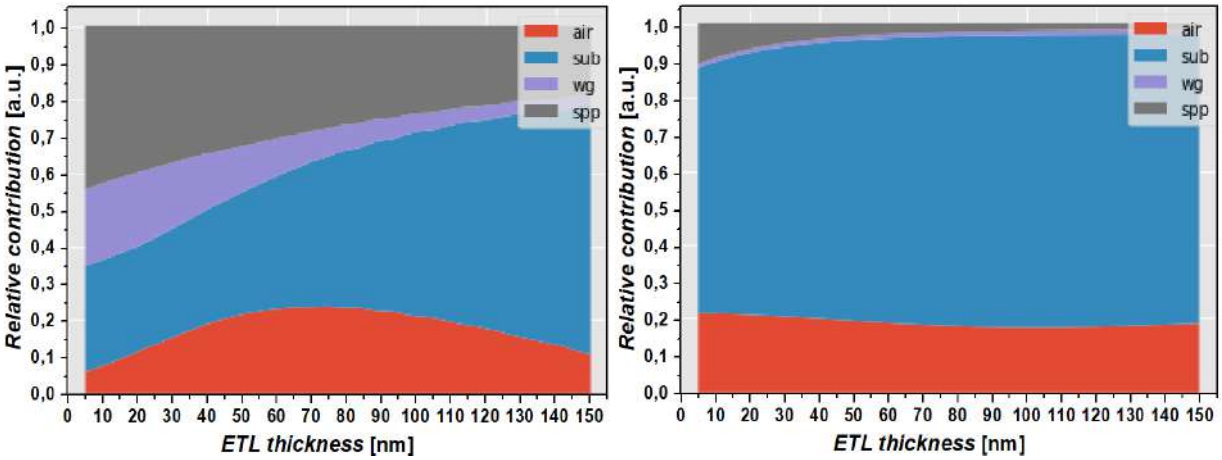

(a)

(b)

**Figure 5:** (a) 2D OLED simulation of the stack as presented in figure 1 showing large losses due to SPP at thin ETLs; (b) 2D OLED simulation of the stack as presented in **Figure 1** replacing the Al electrode with PEDOT:PSS resulting in an independence of ETL thickness and a constant outcoupling to air.

The device, as presented in **Figure 1**, was used for the first simulation (**Figure 5a**), resulting in a poor relative outcoupling to air about 6%. This simulation suggested a 70 nm ETL to achieve a higher outcoupling to air of just over 20%, instead of the used 10 nm. However, this is undesirable as the ETL has a high resistance, thus resulting in much lower efficiencies with fewer charge recombinations being facilitated within the emissive layer.

Furthermore, at this thin ETL, significant losses were linked to the substrate, WG modes, and SPP. Thinner parylene-C substrates should result in fewer absorption losses but would be unsuitable for supporting free-standing OLEDs. Thinner OLED layers would decrease the WG losses due to less TIR at the varying interfaces; however, even thinner layers would hamper efficient PLQY and charge recombinations. At a thin ETL, the Al electrode is close to the emissive layer, making the conditions for SPP easily achievable, resulting in these significant losses.

Preventing these losses due to SPP at thin ETLs was prioritized, from which the idea emerged to replace the Al-electrode with an organic substitute, PEDOT:PSS. A second series of simulations, in which PEDOT:PSS replaced the Al-electrodes, in **Figure 5b** showed an improvement in the relative outcoupling to air. The simulation output suggested an almost complete mitigation of losses due to SPP whilst reducing WG losses, resulting in a relative outcoupling to air of above 20%. Furthermore, ETL thickness dependency diminished significantly. These promising indications by the simulations were attempted to be implemented so that these OLEDs could result in higher EQEs, as shown in the following section.

## 2.7 Performance improvements

To improve the EQEs of these OLEDs, multiple factors were considered that could induce these losses. This wide range of factors included charge trapping at parylene-C - PEDOT:PSS interface, variations in the work function of PEDOT:PSS, interactions with oxygen in- and outside glovebox degrading SY, and inhomogeneities in parylene-C substrate. These potential problems cannot easily be mitigated, but other problems like low PEDOT:PSS electrode conductivity and the aforementioned SPP can be tackled.

### 2.7.1 Conductivity improvements

A trade-off was made by implementing a thicker PEDOT:PSS electrode that can provide a much lower resistance at the cost of slightly lower light transmission. This could be achieved via either spin coating at a lower rotational speed or spin coating multiple subsequent layers [40]. Stacking multiple PEDOT:PSS layers were preferred as the former is linked to a general loss in film homogeneity, which is detrimental to the device's performance. The bottom electrodes received the standard procedure; however, after spin coating, the films were annealed for 5 minutes at 120°C. Subsequently, 100 µL of PEDOT:PSS was again administered to each of the four electrodes before spin coating. The final stacked layer was annealed for 15 minutes at 120°C, during which post-treatment with either methanol or DMSO was performed.

No significant changes to EQE and IV characteristics were observed (**Figure 6**) by implementing these thicker PEDOT:PSS electrodes. The average EQE for methanol-treated devices remained at almost 0.45% while DMSO-treated pixels showed a slightly reduced EQE of, on average, 0.57% (**Figure 6a**). On average, the EQEs did not improve significantly, which could be attributed to the trade-off in improved conductivity to slightly lower light transmission. However, the DMSO-treated devices showed a few pixels with EQEs that exceeded 1,2%. Meanwhile, the methanol-treated devices did not have EQE values above 1%, as observed previously

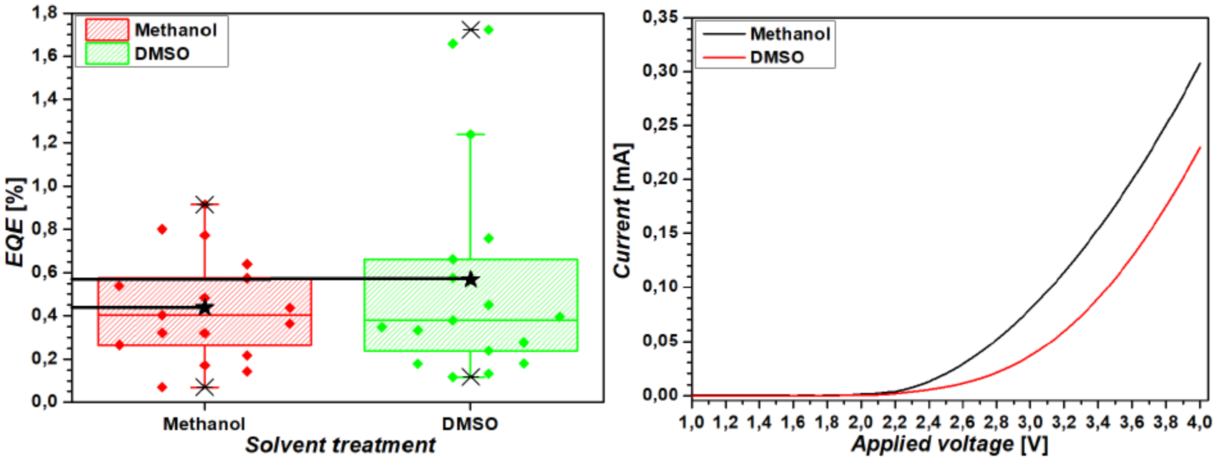

(a) (b)

**Figure 6:** (a) Boxplot of EQE results for OLED devices with double PEDOT:PSS bottom electrodes treated with either methanol or DMSO. Stars indicate the average EQE values of both solvents. The pixels of 6 methanol-treated devices and 6 DMSO-treated devices were tested, and faulty pixels were omitted from these results; (b) IV curves of methanol- and DMSO-treated pixel, which both had an EQE of 0.4%.

(section 2.4.1). Still, the IV characteristics did show a significant improvement related to the conductivity in the devices (**Figure 6b**). The resistance of methanol-treated pixels decreased to 3.92 kΩ (-92.34%) while DMSO-treated ones showed an improved resistance of 4.29 kΩ (-90.73%). The decreased resistances imply that charges can be far more easily injected. More results are presented in **Appendix C.2**.

### 2.7.2 Electrode replacement

As was mentioned in section 2.6, the simulations suggested that replacing the aluminum electrodes with PEDOT:PSS would prevent SPP losses. Combined with the previous improvements to the conductivity, higher EQEs were attempted to be achieved by substituting these aluminum electrodes. Two methods were attempted to achieve this desired design: via direct- or indirect application. Directly applying PEDOT:PSS was performed via drop-casting PEDOT:PSS on top of the OLED stack whilst on the hotplate at 50°C or 120°C (**Appendix E**). Due to the aqueous nature of the PEDOT:PSS solution, this procedure had to be performed outside the glovebox, resulting in the degradation of SY. This was confirmed by IVL measurements, which showed no conduction or purely Ohmic behavior without any light emission.

The indirect method consisted of initially forming the PEDOT:PSS electrodes separately to transfer these onto the OLED stacks. Two strategies were tested: pattern on separate parylene-C substrate or pattern via PEDOT:PSS free-standing film formation. The former case utilized the procedure used for spin coating the bottom electrodes of the OLED. A preferred top electrode pattern was selectively applied to the parylene-C substrate via a mask during UV-ozone treatment. This patterned substrate could be lifted from the quartz substrate and positioned on top of the OLED stack whilst applying 5 µl of PEDOT:PSS at the positions where the top and bottom electrodes would overlap (**Appendix F**). This technique proves promising as it did not show short-circuiting, but no further measurements were performed. This technique's problems were the required precision, which is difficult to obtain by manual handling inside a glovebox, and the difficulty in making proper connections after completing the device.

The second technique involved forming a free-standing PEDOT:PSS gel film inside a mask (**Appendix F**). A 3D-printed mask with the desired shape would be placed on a hydrophobic surface, e.g., parylene-C, and put on the hotplate for 1 hour at 50-70°C. The PEDOT:PSS solution prefers to minimize the interactions with the hydrophobic surface underneath and will form a free-standing film within the pattern, elevated above the parylene-C film, during which water is evaporated. This free-standing gel could be transferred to the glovebox and onto the OLED stack. Though the technique enabled procedures inside the glovebox, problems occurred with achieving a consistent method to obtain the free-standing PEDOT:PSS gel due to leakages and minimal film stabilities.

# 3 Conclusions

Throughout this thesis, profound research has been done to achieve and prove the concept of free-standing, fully functional, and ultra-flexible OLED devices. Direct control over the thickness of the thin, transparent, and flexible parylene-C substrates was established, and sharply defined PEDOT:PSS patterns, serving as electrodes, could be directly achieved via spin coating from aqueous solutions on the hydrophobic substrates. Consequently, a fully spin-coated, flexible OLED could be obtained directly from solution processing. These OLEDs achieved EQEs of, on average, 0,5%, reaching values of over 2% on some occasions. Moreover, over 30 subsequent voltage cycles, the OLEDs showed degradation, resulting in their EQEs dropping in value down to 60% of their initial EQE. Finally, free-standing devices were improved to provide direct connections and become effectively free-standing, rendering them useable for more extended periods in ambient conditions than the initial free-standing OLED designs. This research has proven that ultra-flexible OLEDs are achievable via simple device architectures and that higher performances are within reach with further research.

# 4 Outlook

Further potential changes to the device could be made to improve the external quantum efficiency of these ultra-flexible OLEDs. Firstly, the prospect of applying PEDOT:PSS top electrodes on these OLED devices is one of the most convenient and easily achievable changes to the device. According to the simulations, although not verified within the scope of this thesis, higher EQEs could be achievable by incorporating these fully organic electrodes instead of the conventional metal ones. Secondly, replacing the emissive layer's fluorescent active material, Super Yellow, with second- or third-generation emissive materials would vastly improve the external quantum efficiency, especially with the option to use deposition via evaporation for such materials.

This thesis shows that starting from these initial promising results, many different routes can be investigated for future ventures for even more performing OLEDs and other devices that could harness this high degree of flexibility to fill niche applications, such as solar cells.

# 5 Experimental details

## 5.1 Fabrication of OLED devices

The OLED devices used throughout this research were constructed layer by layer on a 25mm by 25 mm squared glass substrate. These glass substrates were manually washed with soap and acetone and then immersed in an ultrasonic bath in isopropanol (IPA), followed by demi water for 15 minutes. 300 µl of a 100 mg ml$^{-1}$ polyethylene glycol (PEG2000) solution in demi water was used for static spin coating at 1000 rpm over 60 seconds to obtain a smooth sacrificial layer on the glass substrate. The parylene-C layer was formed on top of the substrates employing chemical vapor deposition (SCS Labcoter 2 (PDS 2010)), during which 4 g of parylene-C pellets (Galentis) would form layers of around 2.5 µm. UV-ozone surface treatment (NOVASCAN PDS series) was combined with evaporation masks on top of the parylene-C films to obtain sharply defined PEDOT:PSS patterns suitable for their use as electrodes. 100 µl of PEDOT:PSS was manually applied to the four hydrophilic areas of the parylene-C film to perform static spin coating at 1500 rpm for 60 seconds. Samples were subsequently annealed at 120°C on a hotplate in ambient air for 15 minutes, during which 15 µl of either methanol or DMSO were administered to each of the four PEDOT:PSS patterns to improve their conductivity. A Super Yellow (Livilux, PDY-132) 5 mg ml$^{-1}$ solution in chlorobenzene was heated to 45°C overnight and mixed on a hotplate in a glovebox. This solution was spin-coated inside a glovebox at 1000 rpm for 60 seconds and subsequently annealed at 50°C for 15 minutes on a hotplate. A PEIE 0.003 mg ml$^{-1}$ in IPA was deposited on the substrate via spin-coating at 5000 rpm for 60 seconds inside a glovebox, followed by annealing at 50°C for 15 minutes on a hotplate in the glovebox. 80 nm aluminum electrodes were applied via chemical vapor deposition (VacTec & Inficon SQC-310) under a vacuum of $2{\cdot}10^{-6}$ Pa on top of the organic layers of the device with a deposition rate of 0.2 to 0.7 Å s$^{-1}$. Free-standing OLEDs were obtained by cutting the side of the glass substrate with a razor blade to separate the top parylene-C film from the bottom. With a pair of tweezers, the device could be lifted off the glass substrate by gently peeling. The first series of free-standing devices utilized tape on the edges of the OLED, onto which silver paste was applied with a pencil (G3692 Acheson Silver DAG 1415, density = 1,63 g cm$^{-3}$, solid phase concentration = 57-59%).

## 5.2 Equipment and measurements

Film conductivities of PEDOT:PSS were obtained via a digital multimeter by positioning the probes at a 1 mm separation on the film surface. Absorption-, reflection spectra, and refractive indices were measured by illuminating the samples with a laser-driven light source. The transmitted and reflected light was collected using integration spheres (Thorlab IS200-4) and was measured with an Avantes multichannel spectrometer. Obtained signals were transformed into usable data using the Avasoft 8 software package. All data was plotted and analyzed using OriginPro software. The thicknesses of all the layers were measured by employing a Bruker DekTak profilometer, and the data was obtained via the DekTakTX software. The IV and EQE characterizations were performed using an in-house 5-probe setup connected to two Keithly 2400 source meters. The control and data analysis were performed via an in-house LabView script, which measured voltage ranges from -0.5V to 5V and pixel area was set at 4 mm$^2$ to calculate the EQEs. Simulations were performed via a Python script written by Dr. John Bangshund (University of Minnesota). The script converted the OLED device to a two-dimensional stack into which white-light-emitting dipoles were positioned with random orientation inside the active layer to calculate the in-plane wavevector for the emitted light within the different layers of the 2D model.

# Acknowledgements

I want to thank everyone in the Organic Opto-Electronics research group at UHasselt for their support and interest over the past year. The motivation and curiosity within this group have been a constant source of inspiration and have significantly contributed to the successful realization of this project.
There are a few individuals I would like to thank, especially for their assistance in helping me tackle specific challenges along the way to completing this thesis.

Firstly, I sincerely thank Sigurd for assisting me with measuring the free-standing devices and providing the crucial feedback necessary to improve the OLED design. Your expertise and willingness to help were invaluable.

Secondly, I am grateful to Aslihan for tirelessly working with me to find the best possible method to apply the PEDOT:PSS top electrode to the OLED. Your assistance was key to achieving fully organic OLEDs.

Thirdly, I thank Xueshi for his support in performing simulations and offering additional insights. Your analytical skills and advice greatly enhanced the depth of my research.

Lastly, I want to extend my heartfelt thanks to Bram and Professor Vandewal for the many truly helpful conversations regarding the content and trajectory of this project. Your guidance and perspectives were instrumental in navigating the challenges of this work.

This thesis would not have been possible without all these individuals' support and encouragement, and I sincerely appreciate their contributions. Thank you all for making this journey a rewarding and fulfilling experience I will cherish for years to come.

# 6 References

[1] Jou, J.-H., Kumar, S., Agrawal, A., Li, T.-H. & Sahoo, S. Approaches for fabricating high efficiency organic light emitting diodes. *Journal of Materials Chemistry C* **3**, 2974–3002 (2015).

[2] Han, C. et al. Advanced Technologies for UHD curved OLED TV. *Journal of the Society for Information Display* **22**, 552–563 (2015).

[3] Choi, M. K., Yang, J., Hyeon, T. & Kim, D.-H. Flexible quantum dot light-emitting diodes for next-generation displays. *npj Flexible Electronics* **2**, (2018).

[4] Kim, C.-H. OLED Opportunity in Healthcare With the Pulse Oximeter. *Society for Information Display* **37**, 14–16 (2021).

[5] Sim, J. H. et al. OLED catheters for inner-body phototherapy: A case of type 2 diabetes mellitus improved via duodenal photobiomodulation. *Science Advances* **9**, (2023).

[6] Murawski, C. & Gather, M. C. Emerging biomedical applications of organic light-emitting diodes. *Advanced Optical Materials* **9**, (2021)

[7] Kim, A., Huseynova, G., Lee, J. & Lee, J.-H. Enhancement of out-coupling efficiency of flexible organic light-emitting diodes fabricated on an MLA-patterned parylene substrate. *Organic Electronics* **71**, 246–250 (2019).

[8] Gasonoo, A. et al. Parylene C-aln multilayered thin-film passivation for organic light-emitting diode using a single deposition chamber. *Electronic Materials Letters* **16**, 466–472 (2020).

[9] Trantidou, T., Prodromakis, T. & Toumazou, C. Oxygen plasma induced hydrophilicity of parylene-C thin films. *Applied Surface Science* **261**, 43–51 (2012).

[10] Calcagnile, P. et al. Parylene C surface functionalization and patterning with ph-responsive Microgels. *ACS Applied Materials & Interfaces* **6**, 15708–15715 (2014).

[11] Horii, T., Li, Y., Mori, Y. & Okuzaki, H. Correlation between the hierarchical structure and electrical conductivity of PEDOT/PSS. *Polymer Journal* **47**, 695–699 (2015).

[12] Lang, U., Müller, E., Naujoks, N. & Dual, J. Microscopical investigations of PEDOT:PSS thin films. *Advanced Functional Materials* **19**, 1215–1220 (2009).

[13] Shi, H., Liu, C., Jiang, Q. & Xu, J. Effective approaches to improve the electrical conductivity of PEDOT:PSS: A Review. *Advanced Electronic Materials* **1**, (2015).

[14] Shahrim, N. A., Ahmad, Z., Wong Azman, A., Fachmi Buys, Y. & Sarifuddin, N. Mechanisms for doped pedot:PSS electrical conductivity improvement. *Materials Advances* **2**, 7118–7138 (2021).

[15] Geng, Q. et al. Phase separation to improve the conductivity and work function of the PEDOT:PSS solution for Silicon Hybrid Solar Cells. *The Journal of Physical Chemistry C* **125**, 26379–26388 (2021).

[16] Lim, K. et al. Improving electrical conductivity of PEDOT:PSS with phase separation by applying electric fields. *Bulletin of the Korean Chemical Society* **39**, 469–476 (2018).

[17] Barmpakos, D., Tsamis, C. & Kaltsas, G. Multi-parameter paper sensor fabricated by inkjet-printed silver nanoparticle ink and Pedot:PSS. *Microelectronic Engineering* **225**, 111266 (2020).

[18] Alemu, D., Wei, H.-Y., Ho, K.-C. & Chu, C.-W. Highly conductive pedot:PSS electrode by simple film treatment with methanol for ITO-free polymer solar cells. *Energy & Environmental Science* **5**, 9662 (2012).

[19] Guziak, M. A. et al. Orientation of conductive polymer pedot:PSS Films prepared under Magnetic Field. *Proceedings of the 12th Asia Pacific Physics Conference (APPC12)* 012051 (2014). doi:10.7566/jpscp.1.012051

[20] Yu, Z., Xia, Y., Du, D. & Ouyang, J. Pedot:PSS Films with metallic conductivity through a treatment with common organic solutions of organic salts and their application as a transparent electrode of polymer solar cells. *ACS Applied Materials &; Interfaces* **8**, 11629–11638 (2016).

[21] Deetuam, C. et al. Electrical conductivity enhancement of spin-coated PEDOT:PSS thin film via dipping method in low concentration aqueous DMSO. *Journal of Applied Polymer Science* **132**, (2015).

[22] Li, Q. et al. Highly conductive pedot:pss transparent hole transporting layer with solvent treatment for high performance silicon/organic hybrid solar cells. *Nanoscale Research Letters* **12**, (2017).

[23] Horii, T., Li, Y., Mori, Y. & Okuzaki, H. Correlation between the hierarchical structure and electrical conductivity of PEDOT/PSS. *Polymer Journal* **47**, 695–699 (2015).

[24] Köhler, A. & Bässler, H. in *Electronic Processes in Organic Semiconductors: An Introduction* **1**, 307–388 (Wiley-VCH Verlag GmbH & Co. KGaA, 2015).

[25] Altazin, S., Penninck, L. & Ruhstaller, B. in *Handbook of Organic Light-Emitting Diodes* 1–21 (Springer, Tokyo, 2018).

[26] Burns, S., MacLeod, J., Trang Do, T., Sonar, P. & Yambem, S. D. Effect of thermal annealing super yellow emissive layer on efficiency of oleds. *Scientific Reports* **7**, (2017).

[27] Gambino, S., Bansal, A. K. & Samuel, I. D. W. Photophysical and charge-transporting properties of the copolymer superyellow. *Organic Electronics* **14**, 1980–1987 (2013).

[28] Snedden, E. W., Cury, L. A., Bourdakos, K. N. & Monkman, A. P. High photoluminescence quantum yield due to intramolecular energy transfer in the super yellow conjugated copolymer. *Chemical Physics Letters* **490**, 76–79 (2010).

[29] Salehi, A., Fu, X., Shin, D. & So, F. Recent advances in OLED optical design. *Advanced Functional Materials* **29**, (2019).

[30] Hong, G. et al. A brief history of oleds—emitter development and Industry Milestones. *Advanced Materials* **33**, (2021).

[31] Wei, Q., Ge, Z. & Voit, B. Thermally activated delayed fluorescent polymers: Structures, properties, and applications in OLED devices. *Macromolecular Rapid Communications* **40**, (2018).

[32] Bauri, J., Choudhary, R. B. & Mandal, G. Recent advances in efficient emissive materials-based OLED applications: A Review. *Journal of Materials Science* **56**, 18837–18866 (2021).

[33] Reichardt, C. & Welton, T. in *Solvents and Solvent Effects in Organic Chemistry* 65–106 (Wiley-VCH Verlag GmbH & Co, 2010).

[34] Mansour, A. E. et al. Conductive polymer work function changes due to residual water: Impact of temperature-dependent dielectric constant. *Advanced Electronic Materials* **6**, (2020).

[35] Kim, W. et al. Polymer bulk heterojunction solar cells with PEDOT:PSS bilayer structure as hole extraction layer. *ChemSusChem* **6**, 1070–1075 (2013).

[36] Sze, P.-W. et al. The investigation of high quality pedot:PSS film by multilayer-processing and acid treatment. *Energies* **10**, 716 (2017).

[37] Salehi, A., Fu, X., Shin, D. & So, F. Recent advances in OLED optical design. *Advanced Functional Materials* **29**, (2019).

[38] Harbecke, B. Coherent and incoherent reflection and transmission of multilayer structures. Applied Physics B *Photophysics and Laser Chemistry* **39**, 165–170 (1986).

[39] Furno, M., Meerheim, R., Hofmann, S., Lüssem, B. & Leo, K. Efficiency and rate of spontaneous emission in organic electroluminescent devices. *Physical Review B* **85**, (2012).

[40] Chakraborty, A. et al. Conductive organic electrodes for flexible electronic devices. *Scientific Reports* **13**, (2023).

[41] Yamaguchi, H. et al. Highly flexible and conductive glycerol-doped pedot:PSS Films prepared under an electric field. *Journal of Electronic Materials* **47**, 3370–3375 (2018).

[42] Gutierrez-Fernandez, E., Ezquerra, T. A. & García-Gutiérrez, M.-C. Additive effect on the structure of PEDOT:PSS dispersions and its correlation with the structure and morphology of thin films. *Polymers* **14**, 141 (2021).

[43] Wang, T., Qi, Y., Xu, J., Hu, X. & Chen, P. Effects of poly(ethylene glycol) on electrical conductivity of poly(3,4-ethylenedioxythiophene)–poly(styrenesulfonic acid) film. *Applied Surface Science* **250**, 188–194 (2005).

# Appendix

## A PEDOT:PSS patterning on parylene-C

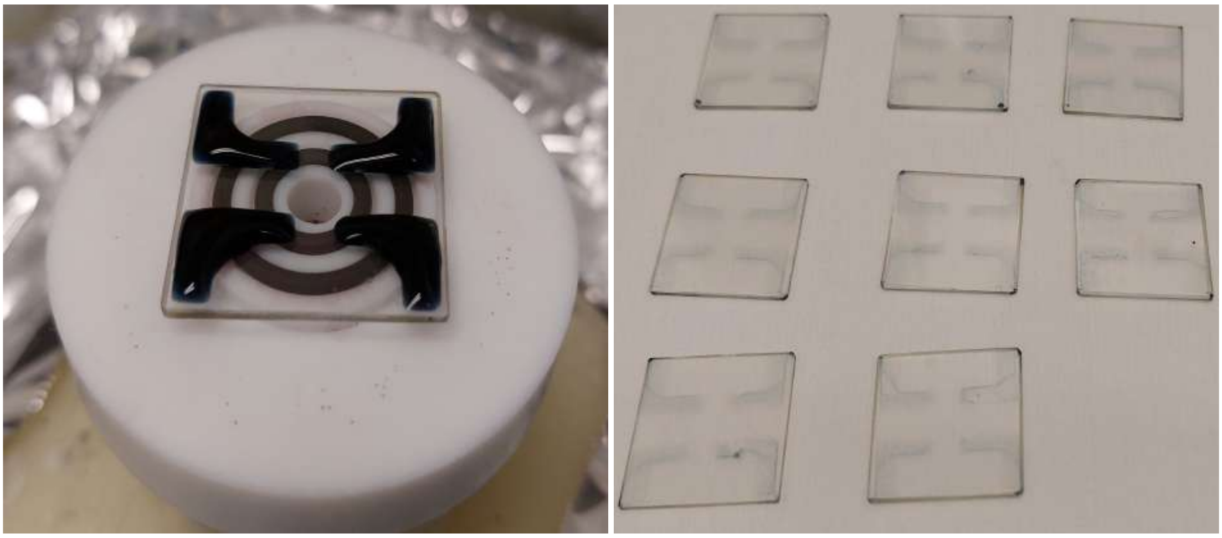

(a)

(b)

**Figure 7:** (a) Confinement of PEDOT:PSS on top of UV-ozone treated areas of the parylene-C film before spin coating, (b) Resulting PEDOT:PSS bottom electrodes after spin coating and conductivity treatment.

# B PEDOT:PSS modifications


(a)
(b)

**Figure 8:** Spin coating of PEDOT:PSS mixed with (a) DMSO resulted in rough film morphology, and (b) glycerol resulted in smooth film morphology.

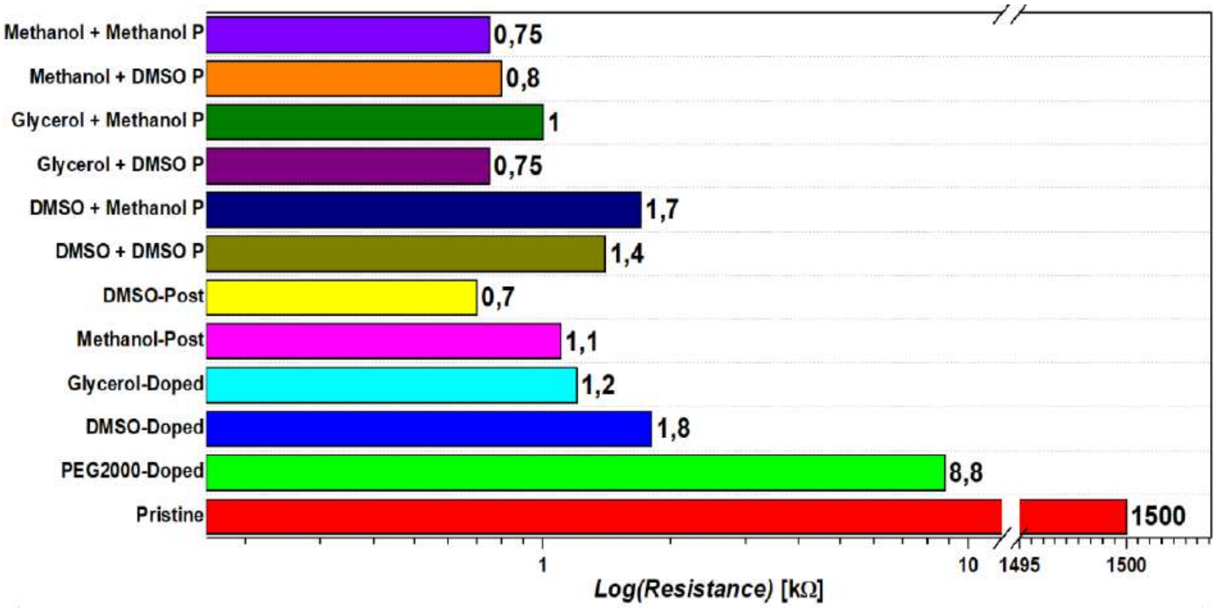

**Figure 9:** PEDOT:PSS conductivity results for one or two treatment methods on the same PEDOT:PSS films. Solvents mentioned with the capital P refer to the solvent being used in post-treatment, and the solvents without this "P" indicate the mixing of this solvent with PEDOT:PSS before spin coating. PEDOT:PSS solutions were prepared by adding different solvents in specific concentrations, values obtained from literature, and mixing them with a vortex (VWR analog vortex mixer): 5 vol% DMSO [20–23 , 5 vol% glycerol [,41 or 2 vol% PEG2000 [.42,43 All PEDOT:PSS solutions were spin-coated at 1500 rpm for 60 seconds in ambient air

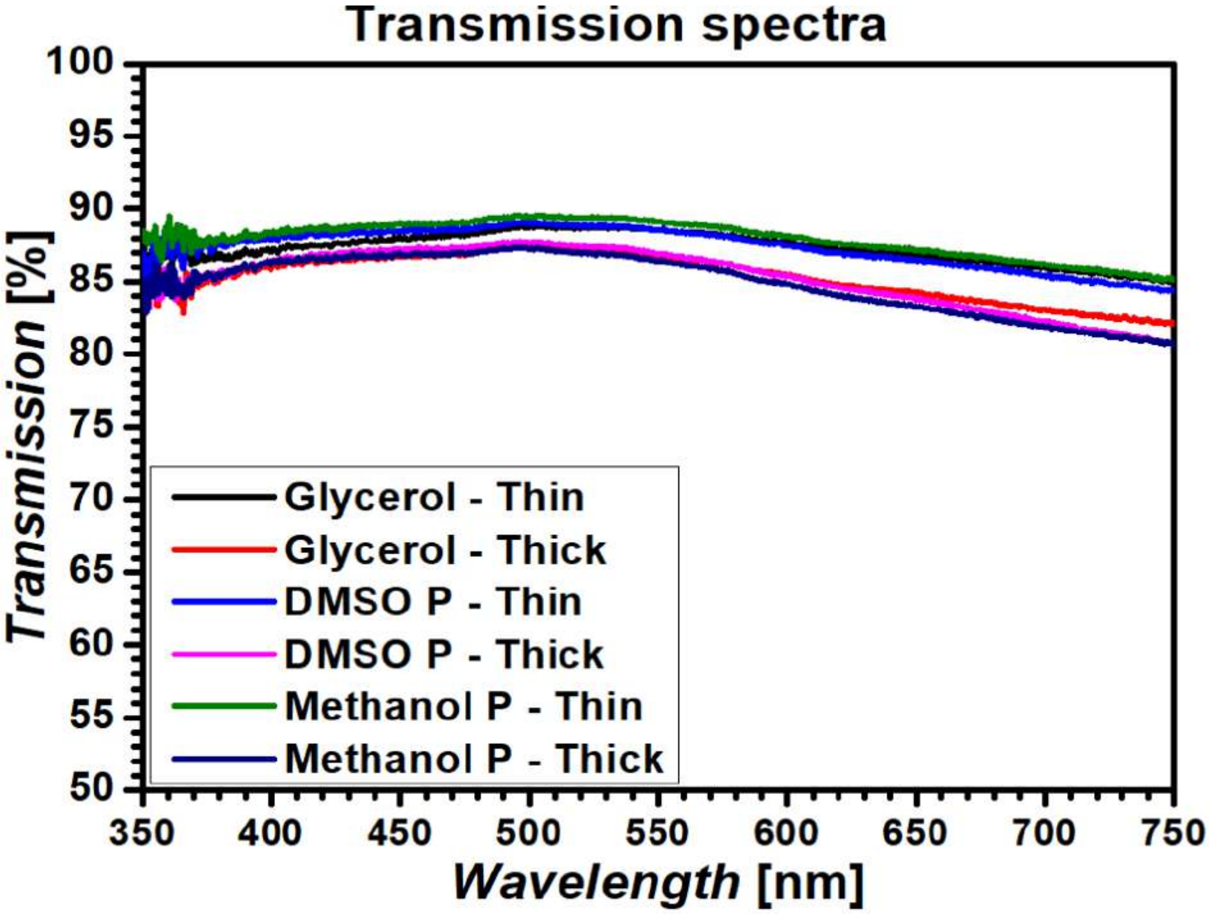

**Figure 10:** Transmission results for varying thicknesses and treatments of PEDOT:PSS on quartz glass substrates. Thick films are around 110 nm, via spin coating at 1000 rpm, and thin films are around 50 nm, via spin coating at 3000 rpm. The P indicates that post-treatment had been used for these substrates.

# C OLED Characterization

## C.1 First series IV characterization

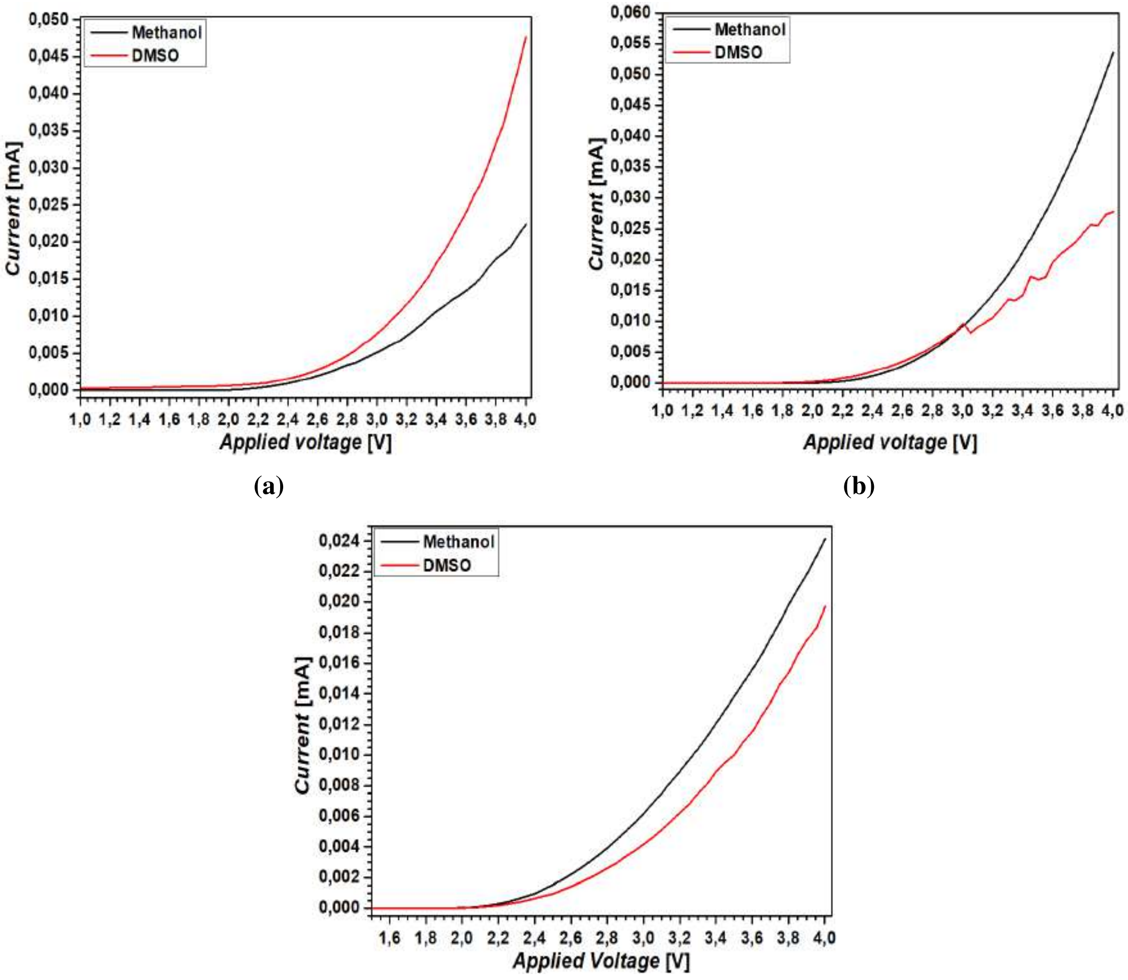

(a)

(b)

(c)

**Figure 11:** IV characteristics of three more first series OLED device pixels at equal EQEs: (a) EQE = 0.25%, resistance methanol = 51.78 kΩ, resistance DMSO = 20.32 kΩ; (b) EQE = 0.35%, resistance methanol = 19.98 kΩ, resistance DMSO = 45.59 kΩ; (c) EQE = 1.1%, resistance methanol = 54.07 kΩ, resistance DMSO = 62.49 kΩ.

## C.2 Second series IV characterization

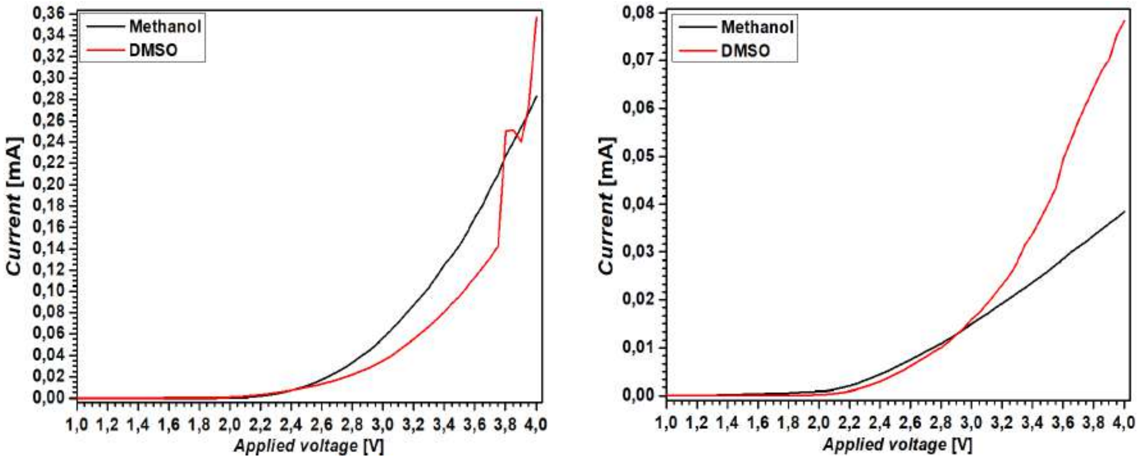

**(a)** **(b)**

**Figure 12:** IV characteristics of two more second series OLED device pixels at equal EQEs: (a) EQE = 0.45%, resistance methanol = 4.03 kΩ, resistance DMSO = 2.01 kΩ; (b) EQE = 0.75%, resistance methanol = 42.25 kΩ, resistance DMSO = 13.91 kΩ.

# D Free-standing OLEDs

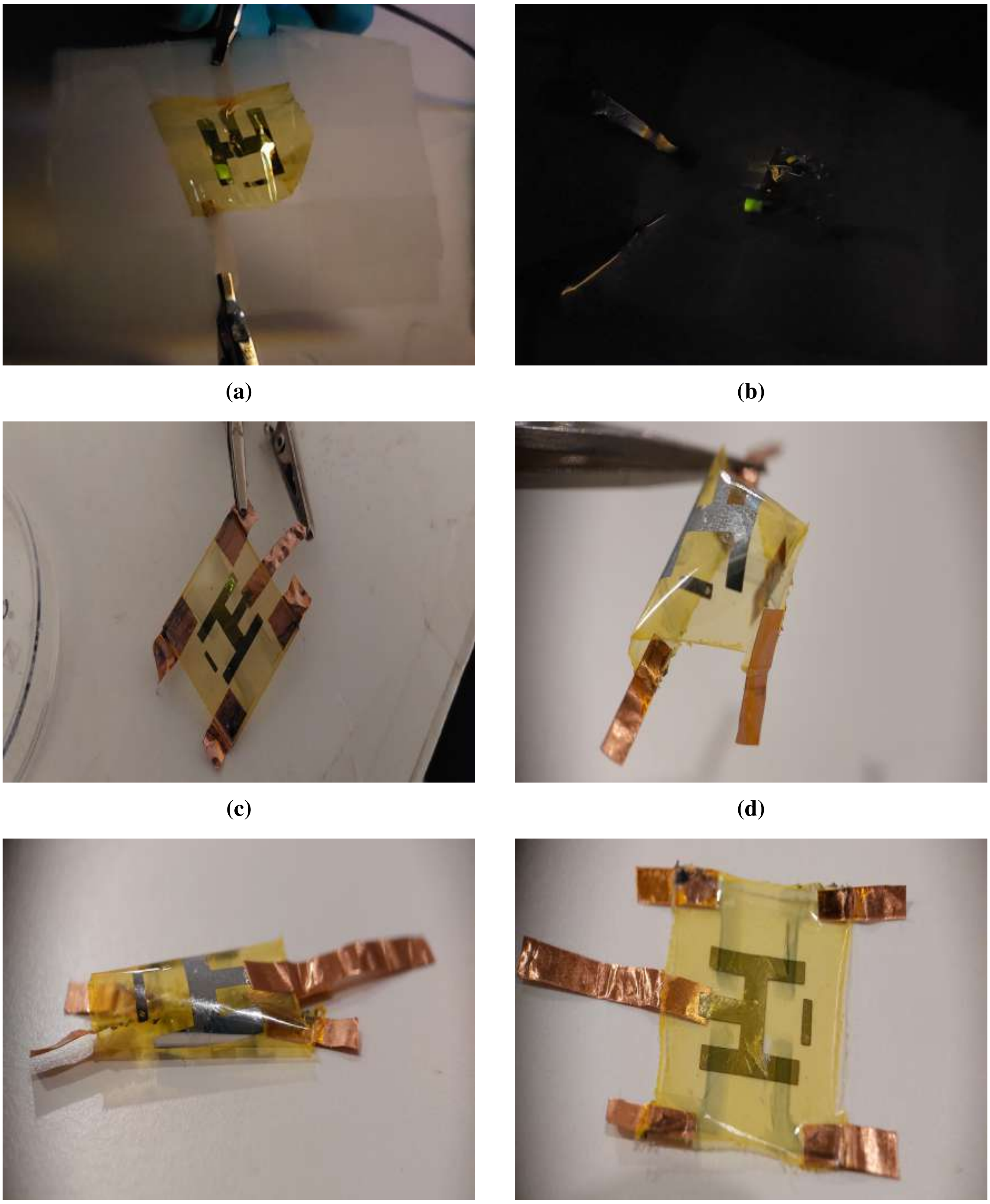

(a) (b) (c) (d) (e) (f)

**Figure 13:** Pictures of free-standing OLED devices, (a) & (b) presenting the first series of these devices to which external connections had been made via silver paste and tape, (c) - (f) show the second series of OLED devices with integrated copper connections.

# E Direct top electrode replacement

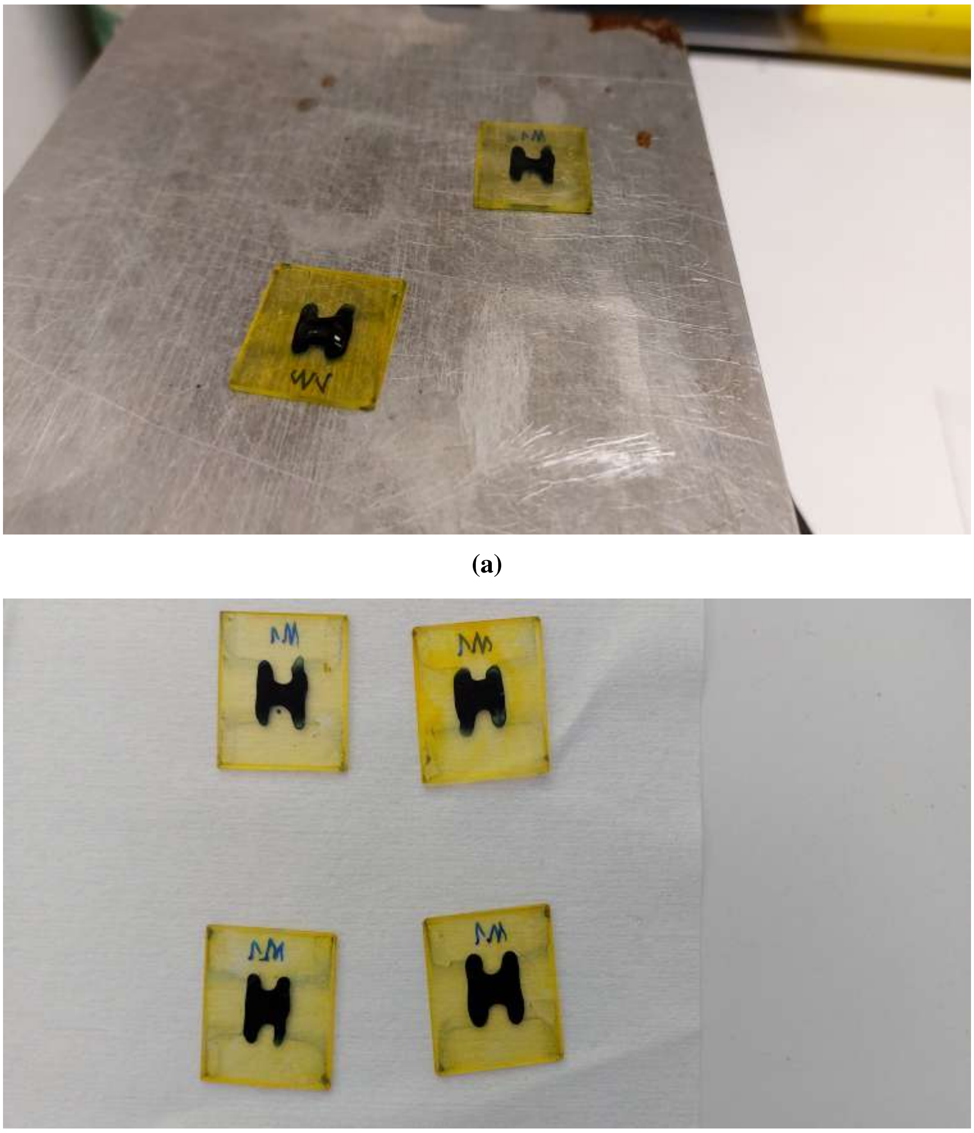

**(a)**

**(b)**

**Figure 14:** (a) Annealing of drop-casted PEDOT:PSS solution in a specific pattern on OLED stacks on hot plate; (b) Results of annealing OLEDs with PEDOT:PSS top electrodes at different temperatures, 120°C (left) showed clear signs of degradation in the form of decoloration. The samples annealed at 50°C (right) did not show such signs.

# F Indirect top electrode replacement

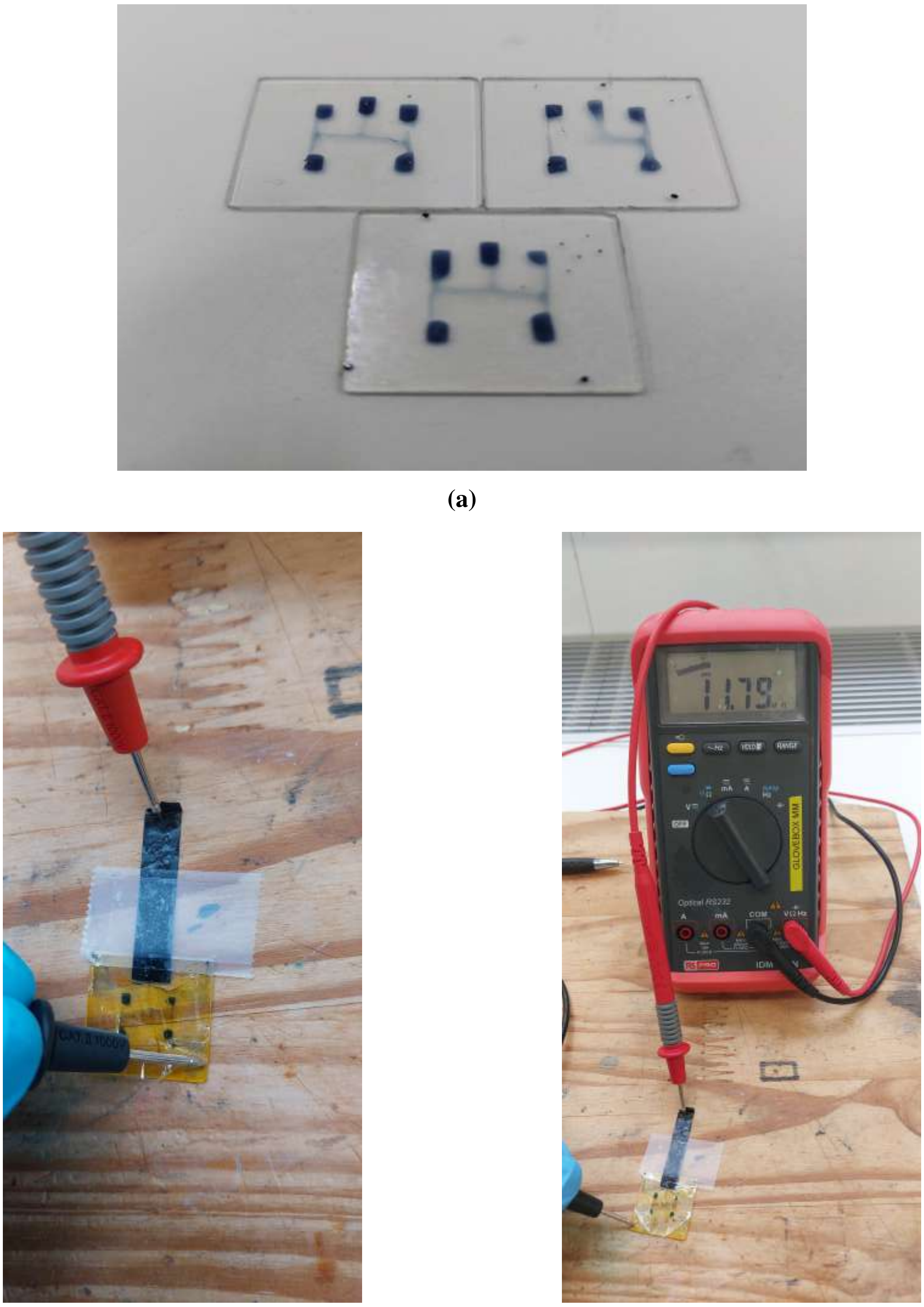

(a)

(b)

(c)

**Figure 15:** (a) Resulting PEDOT:PSS top electrodes on parylene-C after spin coating and annealing; (b) test OLED with the inverted electrode on top and carbon strip to provide connection to the top electrode; (c) full setup showing multimeter indicating no short circuit, but still a conducting path.

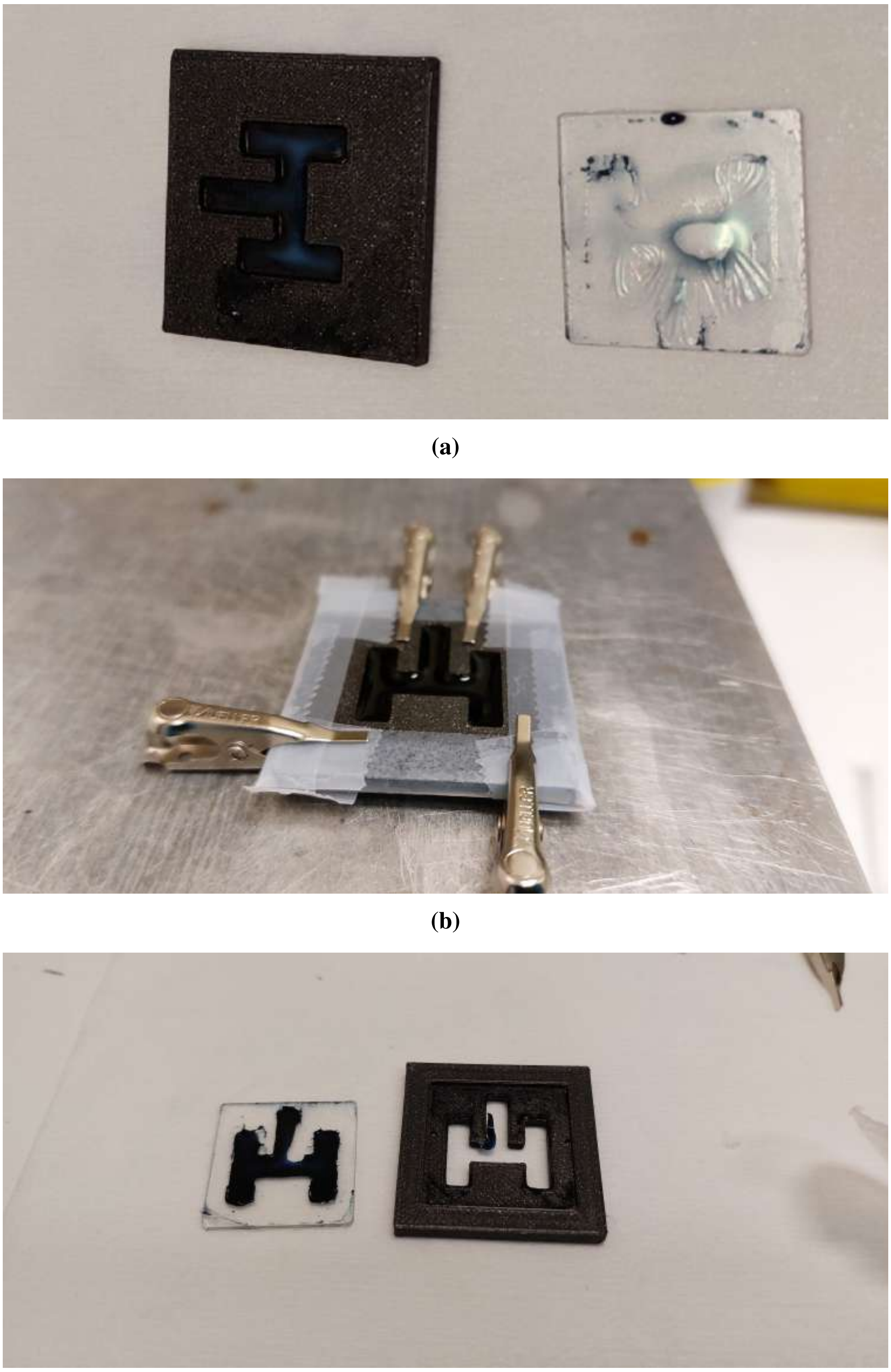

(a)

(b)

(c)

**Figure 16:** (a) Free-standing PEDOT:PSS gel-film inside 3D-printed PET mask next to the used parylene-C-covered quartz substrate after gel formation of 1 hour was finished (b) PEDOT:PSS gel formation on a hotplate at 70°C, covered in tape and clamps to prevent leakages; (c) Transferred PEDOT:PSS pattern onto parylene-C substrate to test procedure.